Materials Physics and Mechanics 47 (2021) 780-786
Research article

Received: June 28, 2021
Accepted: November 4, 2021

FAILURE ANALYSIS IN LIFETIME ESTIMATION OF RAILS

S.A. Atroshenko[1]✉, S.S. Maier[2], V.I. Smirnov[2]

[1]Institute for Problems in Mechanical Engineering, Bolshoy Prospect V.O., 61, St. Petersburg 199178, Russia

[2]Petersburg State Transport University, Moskovsky prospect, 9, St.Petersburg 1900031, Russia

✉ satroshe@mail.ru

Abstract. An attempt is made to find the relationship between the mechanical properties of the material in microvolumes and the properties of the material under load. A fractographic analysis of the surface of a fatigue fracture of a railway rail with an internal transverse crack is presented. The relationship of fractographic features with the structure of the material is discussed.

Keywords: rail steel, fracture surface, recrystallization

Acknowledgements*. No external funding was received for this study.*

Citation: Atroshenko S.A., Maier S.S., Smirnov V.I. Failure analysis in lifetime estimation of rails // Materials Physics and Mechanics. 2021, V. 47. N. 5. P. 780-786. DOI: 10.18149/MPM.4752021_11.

1. Introduction

Due to the increase in the volume of freight and passengers and the intensity of traffic, the risk of rail failure increases, so the analysis of the destruction of deformation changes in the structure of rails after a long-term operation is relevant. Thermo-mechanical damage according to [1] occurs when the wheels slip on the rail. As a result, the rail surface is heated to a high temperature and cooled, which leads to a change in the microstructure and the appearance of microcracks, which causes the generation of transverse fatigue cracks. The onset of defect formation is the occurrence of an internal longitudinal crack from the rail surface. The development of a longitudinal crack leads to the formation of a transverse crack as shown in [2-4]. With small size and large depth, such cracks are not detected by flaw detectors.

When planning the work of flaw detection tools, it is important to know how quickly a transverse crack develops under load and with a different crack surface area. To establish the cause of the break in the rail, a 1.2 m long sample was cut with a crack in the middle. Next, the sample was bent in a three-point pattern with the head down until the sample was divided into parts. After that, a thin section about 1.5 cm thick was cut for metallographic examination of the crack surface and cross-section structure.

2. Material and research technique

The study of the destroyed steel rail, which worked when switching the arrow, was carried out. The studies were carried out on differentially heat-strengthened [5-10] old-year railway rails of the P65 type; passed tonnage – approximately 360 million tons (secondary tracks); manufacturer – Nizhniy Tagil Metallurgical Plant. Samples of P65 rail steel, the properties and elemental composition of which are governed by GOST R 51685-2013, were used as the study material. The chemical composition of this steel (in %) and the mechanical properties

http://dx.doi.org/10.18149/MPM.4752021_11

are as follows: C=0.71-0.82; Mn=0.75-1.25; Si=0.25-0.60; V=0.03-0.15; Cr=0.2-0.8; P≤0.020; S≤0.020; Al≤0.004; UTS≥1180 MPa; $\sigma_{0,2}$≥800 MPa; δ≥8%; φ≥25%; KCU≥250 KJ/m^2. The percentage of the viscous fracture component S (shear area) (in %) was determined according to the ASTM E 436-03. The fracture surface was studied using an Axio Observer Z1-M microscope in a dark field at a magnification of 100X, and the microstructure of the cross-section was analyzed in a bright field using the same microscope and with the help of scanning electron microscope Phenom with microanalyzer. Microhardness was measured on a SHIMADZU instrument brand HMV-G.

3. Results and discussions

A general view of the fracture surface is shown in Fig. 1.

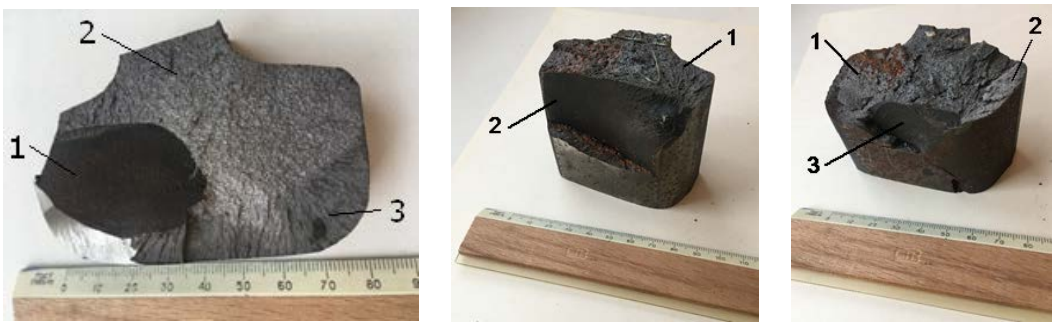

a b c

Fig. 1. View of fracture rail fracture surface: a – *rail_a*, b – *rail_b*, c – *rail_c*

As can be seen from Fig. 1, three zones stand out on the fracture surface *rail_a*. The fractures of the three zones (*rail_a*) are shown in Fig. 2, and the proportion of the viscous component S (shear area in %) on the fracture surface of these three fracture zones is presented in Table 1.

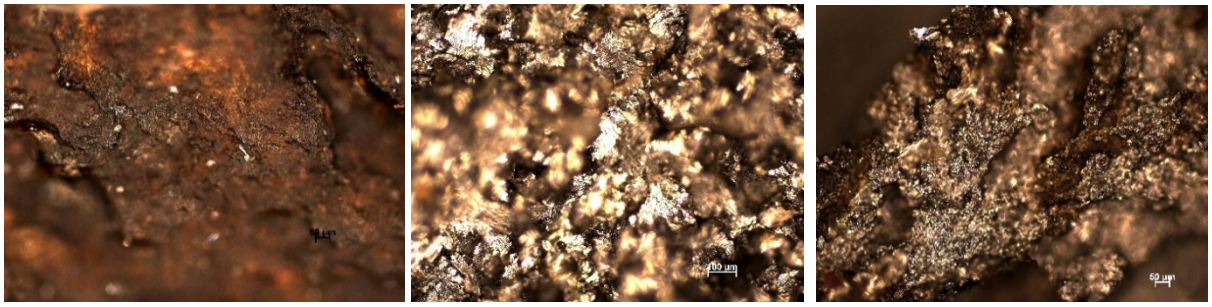

a b c

Fig. 2. Fracture zones (*rail_a*): a – 1, b – 2, c – 3

Two fracture zones of *rail_b* sample are presented in Fig. 3. Three fracture zone in the sample *rail_c* are presented in Fig. 4. The proportion of the viscous component on the fracture surface of fracture zones of these specimens is presented in Table 1.

As can be seen from the data presented, the most brittle failure is observed in the first zone (*rail_a*) – this is the last stage of rail fracture, it begins in the third zone, propagates in the second, and ends in the first, where, in addition to the applied loads, the temperature is also observed similar data in [11]. Samples *rail_b* and *rail_c* with longitudinal cracks have more brittle fracture than specimen *rail_a* with only transverse cracks (Table 1).

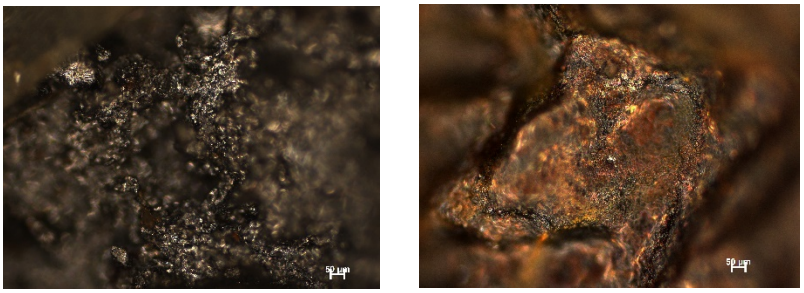

a b

Fig. 3. Fracture zones (*rail_b*): a – 1-transverse, b – 2-longitudinal

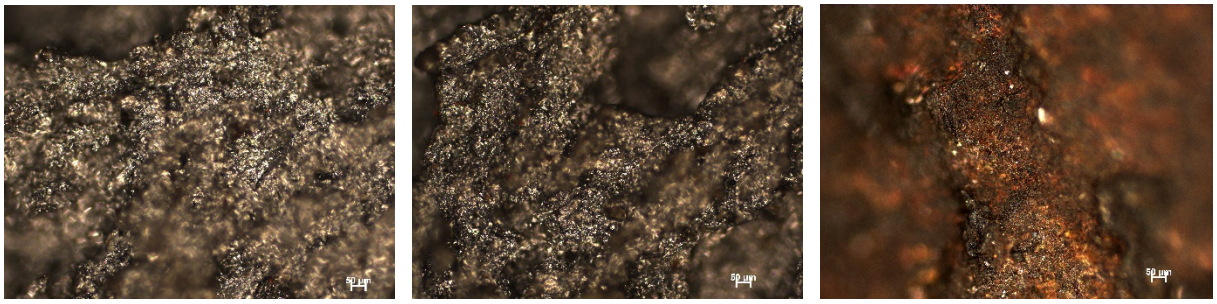

a b c

Fig. 4. Fracture zones (*rail_c*): a – 1-transverse, b – 2-transverse, c – 3-longitudinal

Table 1. The proportion of viscous component S on the fracture surface of rail steel

Sample	Area of fracture	Shear area, S, %
Rail_a	1	96.8
	2	97.4
	3	99.4
Rail_b	1-transverse	98.7
	2-longitudinal	95.7
Rail_c	1-transverse	98.3
	2-transverse	93.1
	3-longitudinal	96.9

Table 2 presents the microhardness of the fracture zones (*rail_a*). The highest hardness was in the middle, most extended fracture zone, and the lowest – in the final, where the sample had already been divided into parts.

Table 2. Microhardness of rail steel in three fracture zones

Area	$HV_{average}$, MPa	Scatter of HV	Deviation, %
1	315.1	300-340	5.7
2	333.3	319-340	2.5
3	315.5	311-322	1.3

An analysis of the microstructure of steel cross-sections in three different fracture areas in the sample *rail_a* showed:

Area 1. The final stage of fracture. In this region near the fracture surface, the structure has a flow pattern, where all structural components are mixed (Fig. 5a), and there is also a branched network of microcracks (Fig. 5b).

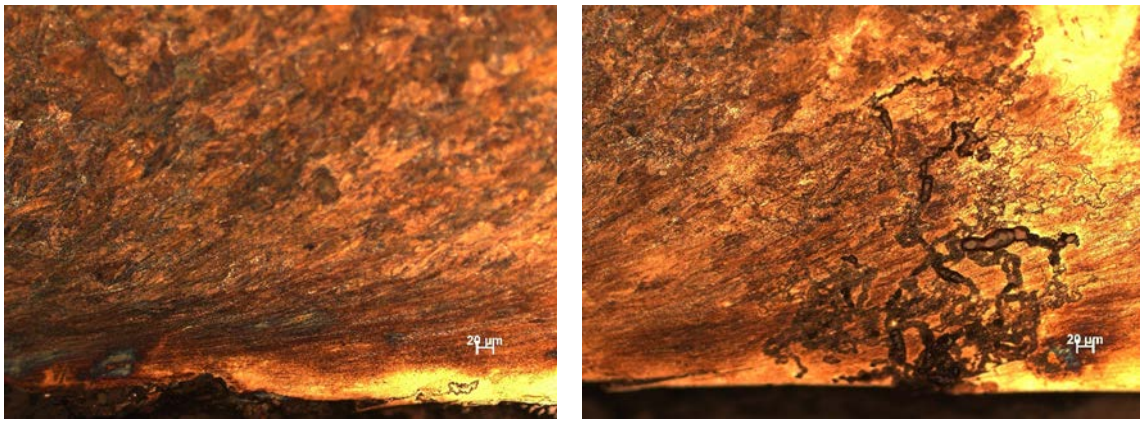

a b

Fig. 5. Microstructure at the fracture surface of region 1 (×200)

In the center of this region (Fig. 6a), a plate-perlite structure typical for this steel is observed, as well as regions of dynamic recrystallization (Fig. 6b), which are often observed under dynamic loading similar to those which were revealed Atroshenko [12].

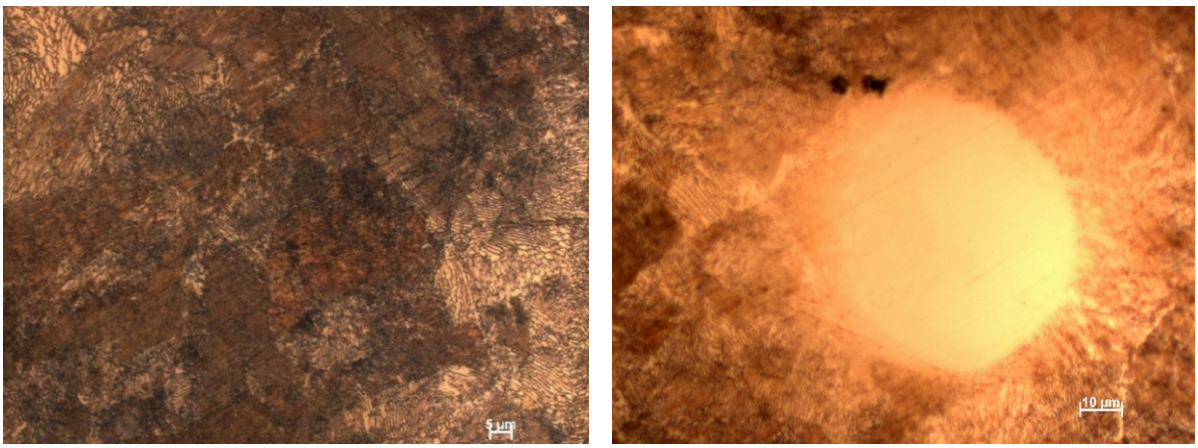

a b

Fig. 6. Microstructure in the center of the region 1 (×1000)

As a result of heating and rapid cooling in these areas of dynamic recrystallization, a microcrystalline structure is observed up to the nanostructure. In some areas of these regions, grain has already grown to 4 μm. As a result of strong heating, annealing occurred in some areas, and lamellar cementite turned into globular, and sometimes it dissolves similarly data of work [13]. If in the third region with which crack initiation and fracture began, the size of the grain and structural components – cementite and ferrite – was smaller (Table 3) then in the second region, these values increased, and in the first area, they were maximum.

Table 3. Quantitative characteristics of the microstructure of rail steel in three areas of fracture

Area	Grain size, μm	Ferrite plate thickness, μm	Cementite plate thickness, μm
1	28.89	1.24	0.18
2	22.57	0.87	0.11
3	5.75	0.72	0.07

Area 2. The intermediate stage of fracture. The onset of an internal longitudinal crack defect is microcracks from accumulations of nonmetallic inclusions elongated during rolling in the form of path lines, which are visible in the microstructure photo (Fig. 7a).

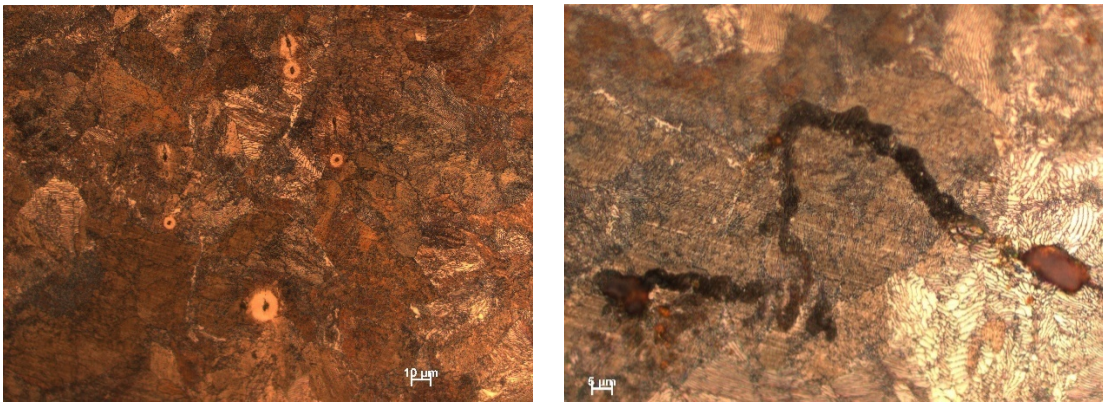

a b

Fig. 7. The origin of microcracks from lines along the rolling (a ×500) and microcracks (b ×1000)

Area 3. The initial stage of fracture. The structure of the initial fracture region is lamellar perlite with a rather fine grain (Table 3) (Fig. 8), in some places of which there are emerging microcracks along the lines from rolling (Fig. 8b).

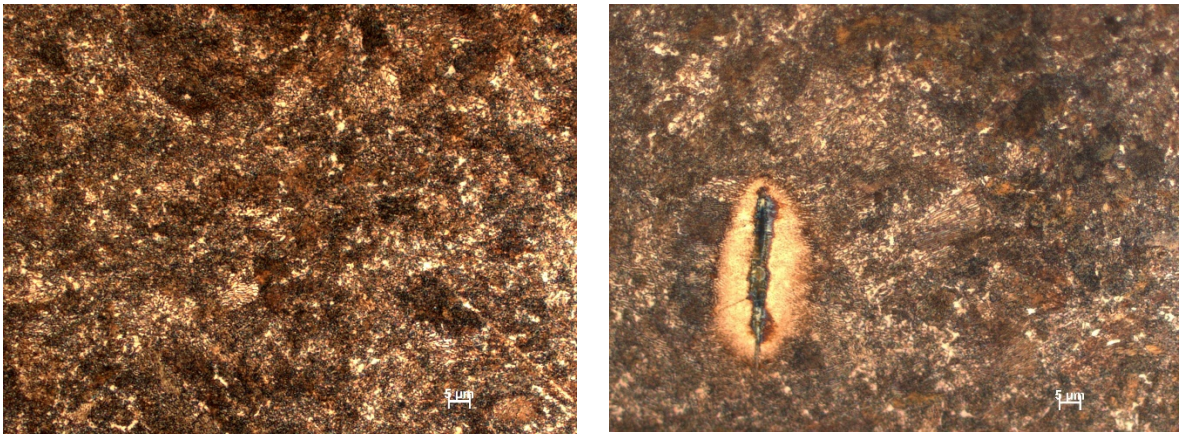

a b

Fig. 8. Steel structure in the central fracture region (×1000)

4. Conclusion

On the fracture surface of the rail, three areas were revealed that differ in brittleness (% fiber on the fracture surface) - the most brittle fracture is observed at the last stage of the fracture of the rail, where, in addition to the effects of loads, the metal is heated.

The highest strength (microhardness) is observed in the middle, most extended fracture region, which is little correlated with the Hall-Petch law, according to which the greatest strength should be in the initial stage of fracture, where the grain size is minimal.

At the final stage of fracture, the nature of the deformation has the features of a wave flow with a network of microcracks from the fracture surface. With the development of fracture, the size of perlite grain increases, as does the size of lamellas of perlite and cementite, and in some places, as a result of significant heating and intense plastic deformation, the fracture of perlite grains occurs, cementite dissolves, and austenite forms, and in some places lamellar perlite becomes globular.

At the final stage of fracture, areas of dynamic recrystallization similar to those observed under shock loading were revealed.

References

[1] Tikhomirov VM. Study of the fatigue strength of a rail with thermo-mechanical damage. *Izvestia TRANSSIBA.* 2013;13: 101-106. (In Russian)
[2] Orringer O, Morris JM. Applied research on rail fatigue and fracture in the United States. *Theoretical and Applied Fracture Mechanics.* 1984;1(1): 23-49.
[3] Orringer O, Morris JM, Jeong DY. Detail fracture growth in rails: test results. *Theoretical and Applied Fracture Mechanics.* 1986;5(2): 63-95.
[4] Kim CS, Chung KW. A Study on Fatigue Crack Propagation of Rail Steel under Constant and Mixed Mode Variable Amplitude Loadings. *IJR International Journal of Railway.* 2012;5(2): 71-76.
[5] Yuriev AA, Gromov VE, Ivanov YF, Rubannikova YA, Starostenkov MD, Tabakov PY. *Structure and Properties of Lengthy Rails after Extreme Long-Term Operation*. Materials Research Forum LLC; 2021.
[6] Gromov VE, Peregudov OA, Ivanov YF, Konovalov SV, Yuriev AA. *Evolution of the structural-phase states of the metal of rails during long-term operation*. Novosibirsk: Publishing house of the SB RAS; 2017. (In Russian)
[7] Gromov VE, Ivanov YF, Yuriev AA. *Differentiated hardened rails: evolution of structure and properties during operation: monograph* Novokuznetsk: Izd. Center SibGIU; 2017. (In Russian)
[8] Gromov VE, Yuriev AA, Peregudov OA, Konovalov SV, Ivanov YF, Glezer AM, Semin AP. Physical nature of structure and properties degradation of rail surface after long term operation. *AIP Conference Proceedings*. 2017;1909(1): 020066.
[9] Gromov VE, Yuriev AA, Ivanov YF, Glezer AM, Konovalov SV, Semina AP, Sundeev RV. Defect substructure change in 100-m differentially hardened rails in long-term operation. *Materials Letters*. 2017;209: 224–227.
[10] Yur'ev AA, Gromov VE, Morozov KV, Peregudov OA. Long-term surface changes in differentially quenched 100-m Rail. *Steel in Translation*. 2017;47(10): 658–661.
[11] Aglan HA, Fateh M. Fracture and fatigue crack growth analysis of rail steels. *Journal of Mechanics of Materials and Structures.* 2007;2: 335-346.
[12] Atroshenko S. Metals dynamic recrystallization up to nanocrystalline size induced shock loading. *AIP Conference Proceedings.* 2016;1748: 030005.
[13] Ivanov YF, Morozov KV, Peregudov, OA, Gromov VE. Operation of rail steel: degradation of the structure and properties of the surface layer. *News of higher educational institutions. Ferrous metallurgy.* 2016;59(8): 576-580.

THE AUTHORS

Atroshenko S.A.
e-mail: satroshe@mail.ru
ORCID: 0000-0002-5733-5915

Maier S.S.
e-mail: sergzo@bk.ru
ORCID: 0000-0003-4917-2578

Smirnov V.I.
e-mail: vsmirnov1@gmail.com
ORCID: 0000-0001-5345-6165